Atmos. Chem. Phys. Discuss., 14, 32393–32425, 2014
www.atmos-chem-phys-discuss.net/14/32393/2014/
doi:10.5194/acpd-14-32393-2014

Atmospheric Chemistry and Physics Discussions
Open Access

Climate extremes in multi-model simulations of stratospheric aerosol and marine cloud brightening climate engineering

V. N. Aswathy[1], O. Boucher[2], M. Quaas[3], U. Niemeier[4], H. Muri[5], and J. Quaas[1]

[1]Institute for Meteorology, Universität Leipzig, Germany
[2]Laboratoire de Météorologie Dynamique / IPSL / CNRS, Université Pierre et Marie Curie, Paris, France
[3]Department of Economics, Christian-Albrechts-Universität zu Kiel, Germany
[4]Atmosphäre im Erdsystem, Max-Planck-Institut für Meteorologie, Hamburg, Germany
[5]Department of Geosciences, University of Oslo, Norway

Received: 2 December 2014 – Accepted: 3 December 2014 – Published: 21 December 2014

Correspondence to: J. Quaas (johannes.quaas@uni-leipzig.de)

Published by Copernicus Publications on behalf of the European Geosciences Union.

Abstract

Simulations from a multi-model ensemble for the RCP4.5 climate change scenario for the 21st century, and for two solar radiation management schemes (stratospheric sulfate injection, G3, and marine cloud brightening, G3SSCE) have been analyzed in terms of changes in the mean and extremes for surface air temperature and precipitation. The climate engineered (SRM 2060s – RCP4.5 2010s) and termination (2080s – 2060s) periods are investigated. During the climate engineering period, both schemes, as intended, offset temperature increases by about 60 % globally, but are more effective in the low latitudes and exhibit some residual warming in the Arctic (especially in the case of marine cloud brightening that is only applied in the low latitudes). In both climate engineering scenarios, extreme temperatures changes are similar to the mean temperature changes over much of the globe. The exception is in Northern Hemisphere high latitudes, where high temperatures (90th percentile of the distribution) of climate engineering relative to RCP4.5 rise less than the mean and cold temperatures (10th percentile) much more than the mean. When defining temperature extremes by fixed thresholds, namely number of frost days and summer days, it is found that both climate engineering experiments are not completely alleviating the changes relative to RCP 4.5. The reduction in 2060s dry spell occurrence over land region in G3-SSCE is is more pronounced than over oceans. Experiment G3 exhibits same pattern as G3-SSCE albeit, stronger in magnitude. A strong termination effect is found for the two climate engineering schemes, with large temperature increases especially in the Arctic. Mean temperatures rise faster than the extremes, especially over oceans, with the exception of the Tropics. Conversely precipitation extremes rise much more than the mean, even more so over the ocean, and especially in the Tropics.

ACPD
14, 32393–32425, 2014

Climate extremes in climate engineering simulations

V. N. Aswathy et al.

1 Introduction

Observed and projected global warming due to continuously increasing greenhouse gas emissions has promoted research focusing on the mitigation of greenhouse gas emissions as well as adaptation to climate change, and lately on alternative methods to counterbalance global warming. Climate engineering or geo engineering has been proposed as a means to counteract global warming in the case mitigation efforts prove insufficient or climate change becomes catastrophic (Crutzen, 2006; Schmidt et al., 2012). There are many proposed methods of climate engineering, which can be classified into two major categories namley Solar radiation management (SRM) and Carbon dioxide removal (CDR). Solar radiation management aims to reduce solar radiation absorbed by the Earth's system by increasing its albedo.

Several SRM techniques are being discussed, among them stratospheric sulfate aerosol injection has been suggested to be most feasible and least expensive (Lenton and Vaughan, 2009; Robock et al., 2009). SRM by marine cloud brightening is another technique, first proposed by Latham (1990).

A number of single model studies have adressed both the SRM techniques (Latham, 2002; Robock et al., 2008; Jones et al., 2009, 2010). Different experiment designs, however, hinder direct model-to-model comparisons (Kravitz et al., 2011). To answer the questions raised in independent studies, a suite of standardized climate modelling experiments has been performed within a coordinated framework, known as the Geoengineering Model Intercomparison Project (GeoMIP). GeoMIP consists of four solar climate engineering experiments namely G1,G2, G3 and G4 (Kravitz et al., 2011), in which the G3 and G4 experiment investigate the effects of stratospheric sulfate aerosol injections. Similarly a first multi-model approach with common experimental setup to study sea salt climate engineering (SSCE), i.e. marine cloud brightening, has been performed within the "Implications and risks of engineering solar radiation to limit climate change" (IMPLICC) project (Alterskjær et al., 2013).

ACPD
14, 32393–32425, 2014

The objective of this paper is to examine multi-model simulation results in terms of changes in mean and extreme temperature and precipitation as a consequence of reducing incoming solar radiation at the surface by these two different SRM techniques. We compare the impact of stratospheric sulfate injection and sea salt climate engineering on change in certain climate extremes. For statospheric sulphate injection, we use the GeoMIP G3 experiment, in which stratospheric aerosols are added gradually to a background of RCP4.5, to balance the anthropogenic forcing and to keep the global temperature nearly constant (Kravitz et al., 2011). The IMPLICC G3-SSCE is based on the GeoMIP G3 experiment, but sea salt emissions by which marine cloud brightness is altered, rather than stratospheric aerosols, are used to compensate the anthropogenic forcing. Since this experiment is based on the GEOMIP G3 experiment, as described in Alterskjær et al. (2013), we denote the experiment G3-SSCE. The stratospheric sulfate experiment, G3, employs the forcing globally, whilst the sea salt climate engineering in G3-SSCE is employed only over tropical oceans.

Kharin et al. (2007) found that the changes in temperature extremes can be expected to generally follow changes in mean temperatures in many parts of the world. However, especially over mid and high latitudes, temperature extremes may show larger relative changes, and over land models show an increase in temperature variability in a warming climate (Kharin and Zwiers, 2005). According to the recent IPCC report, there will be more hot and fewer cold temperature extremes as well as a likely increase in precipitation extremes in a warmer world (Collins et al., 2013).

The climatic properties of the G3 and G3-SSCE experiments have been presented in previous studies. These focused mainly on the temporal and spatial distributions of climate engineering effects on the mean climate (Schmidt et al., 2012; Alterskjær et al., 2013; Kravitz et al., 2013). Schmidt et al. (2012) studied the responses of four Earth system models to climate engineering in the G1 scenario. In this scenario, the radiative forcing from quadrupling of CO_2 is balanced by reducing the solar constant. Alterskjær et al. (2013) investigated the simulation of G3-SSCE. Their results showed that a sufficiently strong application of SSCE led to the compensation of the global annual mean

ACPD
14, 32393–32425, 2014

warming by RCP4.5 in all models. The models showed a suppression of evaporation and reduced precipitation over low-latitude oceans and vice-versa over low-latitude land regions. Kravitz et al. (2013) summarized the current knowledge as gained from the GeoMIP simulations and remaining research gaps. They found that none of the participating models could maintain both global-mean temperature and precipitation to pre-industrial levels from a high CO_2 scenario, in agreement with theoretical considerations.

Presently, very few studies address the impact of climate engineering on extreme events and hardly any research has yet focused on more realistic scenarios. Recent studies by Tilmes et al. (2013) and Curry et al. (2014) examined climate extremes in the multi-model climate engineering experiment (G1). The study by Tilmes et al. (2013) mainly focuses on the hydrological impact of the forcing as applied in the G1 experiment. As part of their study, they also analyze the upper percentile shifts in the annual and seasonal precipitation from monthly averaged model output in both G1 and abrupt 4xCO2 experiments relative to the pre-industrial control state. In the Tropics, the G1 experiment tends to reduce heavy precipitation intensity compared to the control simulation. Their results showed a weakening of hydrological cycle under G1 experiment.

Curry et al. (2014) examined the temperature and precipitation extremes in the G1 scenario. They were found to be smaller than in the abrupt 4xCO2 scenario, but significantly different from pre-industrial conditions. A probability density function analysis of standardised monthly surface temperature exhibited an extension of the high-end tail over land and of the low tail over ocean, while the precipitation distribution was shown to shift to drier conditions. The strong heating of northern high latitudes as simulated under 4xCO2 is largely offset by the G1 scenario. However significant warming was found to remain, especially for daily minimum temperature compared to daily maximum temperature for the given time period. Changes in temperature extremes were found to be more effectively reduced compared to precipitation extremes.

In our study, we define climate extremes in Table 1 (see Methods described in Sect. 2). Details of the experiments considered in the study, models used and methods

ACPD
14, 32393–32425, 2014

are described in Sect. 2. In Sect. 3, we discuss the geographical distribution of the climate extremes as well as the main differences in climate extremes under the two methods during climate engineering and after its termination. In Sect. 4, we discuss the implication of our results and present the conclusions.

2 Data and methodology

Results from the three Earth system models (ESM) were available for the analysis. The models are the Max Planck Institute for Meteorology ESM (MPI-ESM) (Giorgetta et al., 2013), the Norwegian Climate Centre ESM (NorESM) (Alterskjær et al., 2012) and the Institute Pierre-Simon Laplace ESM (IPSL-CM5) (Dufresne et al., 2013). The atmospheric component of the MPI-ESM lower resolution (MPI-ESM-LR), ECHAM6, runs at a resolution of T63 (triangular truncation at wave number 63 corresponding to approximately $1.9^\circ \times 1.9^\circ$) with 47 vertical levels. The Norwegian Earth System Model1 – medium resolution (NorESM1-M) atmospheric model CAM4-OSLO has a resolution of $1.9^\circ \times 2.6^\circ$ with 26 vertical levels, whilst LMDz representing the atmosphere in the IPSL Earth System Model for the 5th IPCC report – low resolution (ISPL-CM5A-LR) runs at a resolution of $1.9^\circ \times 3.75^\circ$ with 39 vertical levels. The advantage of using models of such different components and resolutions is that the results from the different models are expected to span a large part of the uncertainty range of the results (Kravitz et al., 2013).

The G3 and experiment are compared to the RCP4.5 experiment for the period 2020 to 2070. The representative concentration pathway 4.5 (RCP4.5) is a scenario that stabilizes radiative forcing at 4.5 $W\,m^{-2}$ in the year 2100 (Taylor et al., 2012). The aim of the climate engineering experiments is to balance the excess radiative forcing to remain at 2020 levels implied by the anthropogenic climate change in RCP4.5 after year 2020. In the G3 simulation, this is achieved by prescribing aerosol optical depth (AOD) and effective radius as given in Niemeier et al. (2013) in the stratosphere from an equatorial injection of SO_2 (Kravitz et al., 2011). This is done increasingly in time in order to reflect

ACPD
14, 32393–32425, 2014

enough solar radiation to balance the increasing anthropogenic greenhouse effect. An additional 20 year extension until 2090 is performed to explore the effect of abrupt ceasing of the SRM, which is referred to as the "termination effect" (Jones et al., 2013).

In the G3-SSCE experiment, the globally averaged radiative forcing in RCP4.5 relative to the year 2020 is balanced via marine cloud brightening (MCB) by increasing injections of sea salt into the tropical marine atmospheric boundary layer (Alterskjær et al., 2013). The seeding region chosen for the experiment extends between 30° N and 30° S over oceans. Suitable seeding regions were chosen based on an earlier study by Alterskjær et al. (2012). For a detailed description of the G3-SSCE and experiment design the reader is referred to Alterskjær et al. (2013).

The MPI-ESM performed three realizations for both G3 and G3-SSCE experiments. The NorESM1-M performed two realizations for G3 and G3-SSCE, while IPSL-CM5A has one realisation for each experiment. Based on the time period chosen for analysis, we compute the model statistics for each ensemble member for the models where more than one are available, and then consider the multi-model average. The multi-model mean results are given with an equal weight for all three models (i.e. first taking the ensemble-average for the models where more than one ensemble member was available). Prior to all calculations, all the three models ensembles are re-gridded to a common resolution, choosing the lowest of the model resolutions of $1.9^{\circ} \times 3.75^{\circ}$ (IPSL-CM5A-LR resolution).

2.1 Climate extreme analysis

In this study, climate extremes are defined by the lower and upper percentiles of the temporal distribution at each grid-point, as well as a set of indices defined by the Expert Team of Climate Change Detection and Indices (ETCCDI) (Sillmann et al., 2013). Climate extreme are defined for the time-series of near surface air temperature and surface precipitation flux at individual model grid-points.

The data is provided at a daily resolution, so the sample from which the percentiles are drawn covers approximately 3650 days. The 10th (P10) and 90th (P90) percentiles

ACPD
14, 32393–32425, 2014

are analysed. We also investigate higher percentiles (eg P99), but this only as a land- or ocean average where statistics are large enough (as shown in Table 2). Since we do not deseasonalize the data, the 10th percentile may be regarded as a measure of the winter and 90th percentile that of the summer season.

Daily data for maximum (TX) and minimum (TN) temperature are directly provided from the model. The frost days index (FD) represents the number of days when TN < 0 °C and summer days (SU) define the number of days when TX > 25 °C for the given time period. The consecutive dry days index (CDD) provides the largest number of consecutive days when daily precipitation is less than 1 mm day^{-1} in the analysed time period. The climate extreme values are calculated separately for the RCP4.5 and the two SRM experiments.

To assess the influence of climate engineering on a changing climate, for every climate extreme index analysis, the last ten years of climate engineering (2060 to 2069, referred to as 2060s) are compared with ten-year average RCP4.5 control simulation (2010–2019, 2010s, i.e. the pre-SRM period). The same analysis is conducted for the corresponding RCP4.5 scenario for the same two ten-year periods.

To determine the effect of abrupt ceasing of climate engineering, upper percentile climate indices of both temperature and precipitation for the second decade after termination, i.e. years 2080 to 2089 (referred as 2080s) is compared to the last ten years of climate engineering (i.e., 2060s). A similar analysis is carried out for RCP4.5 as well, to investigate the changes during the same two decades.

Both climate engineering techniques are compared with the RCP4.5 2060s (2060 to 2069) and the values are given in Table 4.

3 Results and discussion

For reference, Tables 2–4 show the changes in globally averaged values of mean and extreme (percentile based method) values of temperature and precipitation and Table 5 shows the globally averaged mean values of other extreme event indices (Sects. 3.2

ACPD
14, 32393–32425, 2014

and 3.3). The tropical region in the table is defined as the area between 30° N and 30° S.

The main aim of the climate engineering experiment is to keep the globally averaged top-of-atmosphere radiative forcing at the RCP4.5 2020 level, hence it does not fully constrain the regional climate characteristics of the variables (Curry et al., 2014). Geographical patterns of the changes in climate despite climate engineering are examined in the following section.

3.1 Percentile based climate extreme analysis

Geographical distributions of mean, 90th percentile (P90) and 10th percentile (P10) of near surface temperature are shown in Fig. 1 for RCP4.5 (left column), G3-SSCE (middle column) and G3 (right column). In these maps and those which follow, regions where the three models (ensemble average for the models that simulated more than one ensemble member) agree on the sign of the change are represented by hatches.

In the RCP4.5 scenario, temperatures are almost everywhere warmer in the 2060s than in the 2010s (Fig. 1), albeit with more warming over land than over ocean Collins et al. (2013). In both SRM scenarios, the three models agree on the positive sign of the temperature change (warming) over the extratropics and higher latitudes of the Northern Hemisphere, and also over much of the Southern Hemisphere. In G3-SSCE, the low latitudes show a very slight warming. The warming is also not completely offset in the extratropics, especially in the Northern Hemisphere, which are simulated to warm by about 1 K. In G3-SSCE, the pattern for the P90 values are similar to those for the mean values, with not much offset of temperature (P90), indicating no shift in the tail of the temperature distribution. In some regions, such as the Arctic, the P90 values change somewhat less than the mean values. In G3, the result is very similar to the G3-SSCE experiment: the P90 changes largely follow the mean changes, except for a better mitigation of the warming in the Arctic for the upper percentile compared to the mean.

ACPD
14, 32393–32425, 2014

At the lower end of the temperature distribution, the 10th percentile increases in both SRM experiments broadly show a distribution of small, positive changes very similar to the mean temperature change patterns, except for the Northern Hemisphere high latitudes. In these, rather than a smaller increase as for the upper percentile, a much stronger increase in temperature (P10) is simulated. This is consistently simulated by all three models. Overall, thus both SRM schemes are simulated to substantially narrow the temperature distribution in the Arctic. This is very likely due to the fact that both climate engineering schemes are solar radiation management approaches, by which only during Arctic day climate change can be mitigated (as seen in the upper percentile), while in polar night, almost no local mitigation is achieved by construction. Warming in the lower tail of the temperature distribution may have important effects in the Arctic.

The conclusion that over much of the globe, the extremes change as the mean for the geoengineering schemes, except for the Arctic region, is clearly visible in the analysis of the geographical patterns, even if in the global mean (Table 2) slight differences are calculated.

Changes in mean and the upper percentile (P90) precipitation are shown in Fig. 2. As documented in earlier studies Govindasamy and Caldeira (e.g., 2000), the RCP4.5 scenario shows an increase in precipitation between the 2060s and 2010s, especially in the equatorial region between 5° N and 5° S. The location of this increase, however, is not robust among the three models. Changes in P90 precipitation in the RCP4.5 scenario are stronger than changes in mean precipitation.

Both SRM schemes show small area averaged changes, with decreases in mean precipitation in the subtropics and Tropics and slight increases elsewhere (Fig. 2 and Table 2). The G3-SSCE differs from G3 experiment also due to the aspect that the precipitation is influenced by the emission of sea salt impacting cloud droplet number concentrations and subsequently precipitation formation in the clouds via the autoconversion process. For both the mean and extreme precipitation, the G3-SSCE experiment shows a rather strong positive anomaly over South-East Asia. The Indian subcontinent

ACPD
14, 32393–32425, 2014

and surrounding regions are found to experience enhanced precipitation rates under the G3-SSCE experiment. In contrast, most of the tropical marine regions, including the ITCZ, Pacific, Atlantic and Indian Oceans show a negative anomaly because of G3-SSCE. In the Amazon rainforest area, G3-SSCE largely produces a negative anomaly in precipitation in accordance with the simulation of Jones et al. (2009) on MCB. As discussed by Niemeier et al. (2013), these changes can be attributed to a reduced vertical motion over the tropical Pacific under in the climate engineering experiments. The mean value for the change in precipitation extremes (90th percentile) over global continents is positive at $+0.08\,\mathrm{mm\,day^{-1}}$, while over oceans it is slightly negative at $-0.01\,\mathrm{mm\,day^{-1}}$, yielding a global-mean change of $+0.02\,\mathrm{mm\,day^{-1}}$ (refer Table 2).

The geographical distributions of the changes in precipitation mean and upper percentiles for the stratospheric climate engineering (G3; right column of Fig. 2) are in general similar to the findings for the G3-SSCE simulations, albeit slightly smaller in magnitude over global continents. When averaging globally, and over oceans in particular, however, the G3 experiment produces more positive precipitation changes both for mean and extremes than the G3-SSCE experiment (Tables 2 and 3).

In Figs. 6–8 the precipitation changes as simulated by the individual models are shown. In the G3 scenario, the tendency of all models to simulate moister equatorial tropics (ITCZ) and dryer sub-tropics is even more evident than for the ensemble mean. In P90, both MPI-ESM and NorESM1-M are consistent in simulating a wetter Eurasian continent and wetter South Pacific Convergence Zone. The signals are similar between mean and upper percentile, but stronger for the upper percentile. In the G3-SSCE, all models widely agree on reduced extreme precipitation over tropical marine regions and moister continents and these factors are prominent in G3-SSCE compared to G3 experiment.

3.2 Changes in dry spells

Dry spells are measured as the number of consecutive dry days (CDD). These are defined as the largest number of days per year in which precipitation is less than

ACPD
14, 32393–32425, 2014

1 mm day^{-1}. In Fig. 3, changes in ten-year-average CDD for RCP4.5, G3-SSCE and G3 are shown for 2060s vs. RCP4.5 2010s. CDD changes show little agreement among the three models, this is because it is derived from the more uncertain daily precipitation.

As expected, the desert regions show the extreme values. RCP4.5 has fewer CDD in the 2060s with a global mean reduction of 1.8 days $year^{-1}$ over land, while over the tropical regions there is an increase in CDD of 1.44 days $year^{-1}$.

In the G3-SSCE experiment, shorter dry periods are simulated, especially over the land regions. Australia, South Africa and most of Asia show a decrease by approximately 2–5 days $year^{-1}$. Over the Arabian peninsula, the decrease in CDD is up to 10 days $year^{-1}$. There are few regions where CDD increases in G3-SSCE, mostly over parts of North Africa including Libya and Algeria. Overall the effect of G3-SSCE is most pronounced over global continents with a reduction of 0.68 days $year^{-1}$. Hence in G3-SSCE, the overall increase in mean and extreme precipitation (discussed earlier) over continent and decrease over oceans is reflected in the CDD values as well. G3 experiment results in increase in CDD, over the Tropics as well as global oceans and, reductions in CDD over large parts of extratropical continents, but more strong in magnitude than the G3-SSCE.

3.3 Changes in frequency of occurrence of cold days and hot days

The frequency of occurrence of cold days can be quantified as the number of frost days, defined as total number of days per year when TN less than 0 °C. In RCP4.5, FD is reduced in the mid- to high latitudes especially of the Northern Hemisphere by up to one month per year, and widespread by 5 and more days per year over all extra-tropical continental areas of the Northern Hemisphere (Fig. 4a).

Globally there is less decrease in the frost days under both SRM scenarios compared to RCP4.5 with mean changes of −3.3, −2.86 and −5.98 days $year^{-1}$ for G3-SSCE, G3 and RCP4.5 respectively (Table 5). RCP4.5 scenario show very few regions of increase

ACPD
14, 32393–32425, 2014

in frost days. In comparison to RCP4.5, the SRM scenarios maintain more frost days over NH land. However, still a strong reduction in the frequency of occurrence of FD is simulated for both G3 and G3-SSCE, with patterns very similar to the simulated increase in the RCP4.5 scenario. It may be concluded that the warming especially of the lower end of the temperature distributions not offset by the SRM scenarios (see above) is sufficiently strong. Hence, it reduces the frequency at which the freezing threshold is reached and subsequently FD reduction is largely not alleviated.

The frequency of occurrence of hot days can be quantified as the number of Summer days (SU) defined as the the total number of days per year in which TX is greater than 25 °C. Figure 5 shows the change in SU for 2060s vs. RCP4.5 2010s. As expected, RCP4.5 shows an increase in SU. This is most pronounced in the sub-tropics with increases by up to more than one month per year, but is widespread over low- to mid-latitude continents. In the Tropics the maximum increase of 118 days $year^{-1}$ corresponds to an entire season more of SU, and the average increase is as much as 26 days $year^{-1}$ (Table 5). This strong increase over the Tropics is well reduced by the G3-SSCE scenario, however, the still substantial increase of 10–20 days $year^{-1}$ over North America and Eurasia is only slightly offset. In contrast, the extra-tropical changes in SU are effectively reduced by the globally-applied G3 scheme, where, in turn, still substantial increases in SU over the Tropics (up to 30 days $year^{-1}$) are simulated.

3.3.1 Termination effect

The termination effect of the G3 and G3-SSCE experiments are investigated for both temperature and precipitation. The values are summarized in Table 3.

As expected, the termination of SRM leads to a rapid net global warming. When following the RCP4.5 scenario (2080s vs. 2060s) a gradual warming is simulated which is stronger for the average temperatures in the northern polar and mid-latitude regions than the global average of +0.26 K. P90 temperatures rise at a slower rate than the average ones, except in the Tropics where the warming rates are slightly larger for the upper percentiles (not shown). The termination of the SRM leads to strong warming

ACPD
14, 32393–32425, 2014

both of average and extreme temperatures for both schemes, with slightly larger values for the G3 simulations. The changes are stronger over land. Mean values rise the most in the northern polar regions, while P90 values increase more at mid- and low latitudes over land, with only moderate warming in the polar regions. The global mean values of the temperature changes for the G3-SSCE scenario for mean, P90 and P99 are +0.73, +0.54 and +0.56 K, respectively (Alterskjær et al., 2013). In the G3 scenario, simulated patterns are similar to G3-SSCE, but stronger. The termination of the SRM leads to stronger changes in extreme temperatures also in the mid- and polar regions, compared to the G3-SSCE method. The global mean change for temperature (P99) extremes over land is +1.13 K. A similar analysis is carried out for precipitation as well. Termination of G3-SSCE leads to strong increases of precipitation over most regions. However, the models simulate drying over some subtropical land regions, namely north of Africa, Australia and some regions of Indian subcontinent due to the termination effect. The global mean change of precipitation extremes is +0.74 mm day^{-1} (P99). Especially the Tropics experience a large increase in precipitation extremes (P99) with a net value of +1.26 mm day^{-1}. Under G3 termination, similar results are found, albeit with less drying anomalies in the subtropical areas.

4 Conclusions

In this study, the results of simulations with three different Earth system models within the SRM climate engineering model intercomparison studies of IMPLICC and GeoMIP have been analyzed with respect to surface air temperature and precipitation and their corresponding extreme indices. Two solar radiation management methods were implemented in these simulations, namely the injection of stratospheric aerosols (G3) and marine cloud brightening by sea salt injections (G3-SSCE). Both solar radiation management climate engineering methods are effective at counteracting the mean global warming caused by the RCP4.5 scenarios. In the marine cloud brightening experiment, G3-SSCE, however, where SRM is implemented only in the Tropics, extra-tropics and

ACPD
14, 32393–32425, 2014

high latitudes warm up during the climate engineered time. The focus of this study was on the changes in extreme temperatures, defined here as the upper (90th, P90) and lower percentiles (10th, P10) of the 10 year temporal distribution at each grid-point, as well as dry-spell, frost-day and summer-day indices. In the simulations investigated, over much of the globe, P90 temperatures change similar to the mean temperatures despite a small global-mean difference in changes. The exception is in Northern Hemisphere high latitudes, where the warm temperatures rise slower than the mean, but the cold temperatures much faster than the mean. This is consistent with the expectation, since SRM is effective only during polar day. Defining temperature extremes by fixed thresholds, namely frost days as those where the minimum temperature is colder than the freezing point, and summer days as those where the maximum temperature is warmer than 25 °C, it is found that neither SRM scheme effectively alleviates the decrease in the RCP4.5 frost days simulated for the mid- and high latitude continental regions, nor the scheme completely offset the increase in summer days. The patterns for the two schemes differ – G3 better reduces the increase in the extra-tropics while G3-SSCE better reduces the increase in the sub-tropics.

In terms of precipitation, it was found that the increases in mean and also P90 precipitation are in general well offset by both schemes. In the Tropics, especially over marine regions, the G3-SSCE scheme leads to an overall reduction in precipitation. The geographical patterns of the P90 precipitation change show large variability which averages out when considering large regions. In G3, consistent among the models is a tendency in the low latitudes to have precipitation more concentrated in the equatorial tropics, indicating an intensification of the ITCZ, and to produce more precipitation over Eurasia. As for dry spells, G3-SSCE produce more reduction over global continents compared to the oceans. G3, in turn shows the same, albeit more strong in the magnitude.

Strong temperature increases are simulated after the ceasing of SRM climate engineering. G3 termination results in a rapid warming of entire globe, stronger over land in both tropical and extra-tropical regions than over oceans, and less strong over the

ACPD
14, 32393–32425, 2014

Arctic for the 20 year timeframe analysed. The G3-SSCE termination effect is more confined to the Tropics. Also precipitation responds strongly to the termination of SRM climate engineering measures with strong increases over land regions. Extreme values, both for temperature and precipitation, show stronger increases than the mean values for the termination effect.

This study has implications for the assessment of social costs of SRM climate engineering. Typically the extreme values of temperature or precipitation give rise to economic damages. Since changes in temperature and precipitation extremes in general are more or less equally affected by the two SRM climate engineering methods as the mean values, there is no substantial indication for costly side effects in this regard, except for the Arctic region. Other non-mitigated costs of greenhouse gas emissions, e.g. sea level rise, ocean acidification, have not been assessed here. Furthermore, some effects are subject to considerable uncertainty, such as the exact geographical pattern of P90 precipitation change.

Acknowledgements. The IMPLICC EU project (grant no FP7-ENV-2008-1-226567) and its researchers (Ulrike Niemeier and Hauke Schmidt, Max Planck Institute for Meteorology, Hamburg; Michael Schulz, met.no Oslo; Kari Alterskjær and Jón Egill Kristjánsson, University of Oslo); and as well as the GeoMIP project are acknowledged for conducting the simulations and providing the model output. This study was supported by the German Research Foundation (Deutsche Forschungsgemeinschaft, DFG) in the Priority Programme (Schwerpunktprogramm 1689 "Climate Engineering – Risks, Challenges, Opportunities?"), project "Learning about cloud brightening under risk and uncertainty: Whether, when and how to do field experiments", GZ QU-311/10-1. The IPSL-CM5A climate simulations were performed with the HPC resources of [CCRT/TGCC/CINES/IDRIS] under the allocation 2012-t2012012201 made by GENCI (Grand Equipement National de Calcul Intensif), CEA (Commissariat à l'Energie Atomique et aux Energies Alternatives), and CNRS (Centre National de la Recherche Scientifique). Helene Muri is funded by the Norwegian Research Council Project EXPECT (grant 229760/E10) and NorESM1-M computing resources was provided by NOTUR and NORSTORE.

References

Alterskjær, K., Kristjánsson, J. E., and Seland, Ø.: Sensitivity to deliberate sea salt seeding of marine clouds – observations and model simulations, Atmos. Chem. Phys., 12, 2795–2807, doi:10.5194/acp-12-2795-2012, 2012. 32398, 32399

Alterskjaer, K., Kristjánsson, J. E., Boucher, O., Muri, H., Niemeier, U., Schmidt, H., Schulz, M., and Timmreck, C.: Sea-salt injections into the low-latitude marine boundary layer: the transient response in three Earth system models, J. Geophys. Res.-Atmos., 118, 12195–12206, doi:10.1002/2013JD020432, 2013. 32395, 32396, 32399, 32406

Collins, M., Knutti, R., Arblaster, J., Dufresne, J.-L., Fichefet, T., Friedlingstein, P., Gao, X., Gutowski, W., Johns, T., Krinner, G., Shongwe, M., Tebaldi, C., Weaver, A., and Wehner, M.: Long-term climate change: projections, commitments and irreversibility, in: Climate Change 2013: The Physical Science Basis. Contribution of Working Group I to the Fifth Assessment Report of the Intergovernmental Panel on Climate Change, edited by: Stocker, T. F., Qin, D., Plattner, G.-K., Tignor, M., Allen, S. K., Boschung, J., Nauels, A., Xia, Y., Bex, V., and Midgley, P. M., Cambridge University Press, Cambridge, UK, New York, NY, USA, 2013. 32396, 32401

Crutzen, P. J.: Albedo enhancement by stratospheric sulfur injections: a contribution to resolve a policy dilemma?, Climatic Change, 77, 211–220, doi:10.1007/s10584-006-9101-y, 2006. 32395

Curry, C. L., Sillmann, J., Bronaugh, D., Alterskjaer, K., Cole, J. N. S., Ji, D., Kravitz, B., Kristjánsson, J. E., Moore, J. C., Muri, H., Niemeier, U., Robock, A., Tilmes, S., and Yang, S.: A multi-model examination of climate extremes in an idealized climate engineering experiment, J. Geophys. Res.-Atmos., 119, 3900–3923, doi:10.1002/2013JD020648, 2014. 32397, 32401

Dufresne, J.-L., Foujols, M.-A., Denvil, S., Caubel, A., Marti, O., Aumont, O., Balkanski, Y., Bekki, S., Bellenger, H., Benshila, R., Bony, S., Bopp, L., Braconnot, P., Brockmann, P., Cadule, P., Cheruy, F., Codron, F., Cozic, A., Cugnet, D., Noblet, N., Duvel, J.-P., Ethé, C., Fairhead, L., Fichefet, T., Flavoni, S., Friedlingstein, P., Grandpeix, J.-Y., Guez, L., Guilyardi, E., Hauglustaine, D., Hourdin, F., Idelkadi, A., Ghattas, J., Joussaume, S., Kageyama, M., Krinner, G., Labetoulle, S., Lahellec, A., Lefebvre, M.-P., Lefevre, F., Levy, C., Li, Z. X., Lloyd, J., Lott, F., Madec, G., Mancip, M., Marchand, M., Masson, S., Meurdesoif, Y., Mignot, J., Musat, I., Parouty, S., Polcher, J., Rio, C., Schulz, M., Swingedouw, D., Szopa, S., Ta-

ACPD
14, 32393–32425, 2014

Climate extremes in climate engineering simulations

V. N. Aswathy et al.

landier, C., Terray, P., Viovy, N., and Vuichard, N.: Climate change projections using the IPSL-CM5 Earth System Model: from CMIP3 to CMIP5, Clim. Dynam., 40, 2123–2165, doi:10.1007/s00382-012-1636-1, 2013. 32398

Giorgetta, M. A., Jungclaus, J., Reick, C. H., Legutke, S., Bader, J., Böttinger, M., Brovkin, V., Crueger, T., Esch, M., Fieg, K., Glushak, K., Gayler, V., Haak, H., Hollweg, H.-D., Ilyina, T., Kinne, S., Kornblueh, L., Matei, D., Mauritsen, T., Mikolajewicz, U., Mueller, W., Notz, D., Pithan, F., Raddatz, T., Rast, S., Redler, R., Roeckner, E., Schmidt, H., Schnur, R., Segschneider, J., Six, K. D., Stockhause, M., Timmreck, C., Wegner, J., Widmann, H., Wieners, K.-H., Claussen, M., Marotzke, J., and Stevens, B.: Climate and carbon cycle changes from 1850 to 2100 in MPI-ESM simulations for the Coupled Model Intercomparison Project phase 5, J. Adv. Model. Earth Syst., 5, 572–597, doi:10.1002/jame.20038, 2013. 32398

Govindasamy, B. and Caldeira, K.: Geoengineering Earth's radiation balance to mitigate CO_2 induced climate change, Geophys. Res. Lett., 27, 2141–2144, 2000. 32402

Jones, A., Haywood, J., and Boucher, O.: Climate impacts of climate engineering marine stratocumulus clouds, J. Geophys. Res., 114, D10106, doi:10.1029/2008JD011450, 2009. 32395, 32403

Jones, A., Haywood, J., Boucher, O., Kravitz, B., and Robock, A.: Geoengineering by stratospheric SO_2 injection: results from the Met Office HadGEM2 climate model and comparison with the Goddard Institute for Space Studies ModelE, Atmos. Chem. Phys., 10, 5999–6006, doi:10.5194/acp-10-5999-2010, 2010. 32395

Jones, A., Haywood, J. M., Alterskjaer, K., Boucher, O., Cole, J. N. S., Curry, C. L., Irvine, P. J., Ji, D., Kravitz, B., Kristjánsson, J. E., Moore, J. C., Niemeier, U., Robock, A., Schmidt, H., Singh, B., Tilmes, S., Watanabe, S., and Yoon, J.-H.: The impact of abrupt suspension of solar radiation management (termination effect) in experiment G2 of the Geoengineering Model Intercomparison Project (GeoMIP), J. Geophys. Res.-Atmos., 118, 9743–9752, doi:10.1002/jgrd.50762, 2013. 32399

Kharin, V. V. and Zwiers, F. W.: Estimating extremes in transient climate change simulations, J. Climate, 18, 1156–1173, 2005. 32396

Kharin, V. V., Zwiers, F. W., Zhang, X., and Hegerl, G. C.: Changes in temperature and precipitation extremes in the IPCC ensemble of global coupled model simulations, J. Climate, 20, 1419–1444, doi:10.1175/JCLI4066.1, 2007. 32396

Kravitz, B., Robock, A., Boucher, O., Schmidt, H., Taylor, K. E., Stenchikov, G., and Schulz, M.: The Geoengineering Model Intercomparison Project (GeoMIP), Atmos. Sci. Lett., 12, 162–167, doi:10.1002/asl.316, 2011. 32395, 32396, 32398

Kravitz, B., Robock, A., Forster, P. M., Haywood, J. M., Lawrence, M. G., and Schmidt, H.: An overview of the Geoengineering Model Intercomparison Project (GeoMIP), J. Geophys. Res.-Atmos., 118, 13103–13107, doi:10.1002/2013JD020569, 2013. 32396, 32397, 32398

Latham, J.: Marine cloud brightening, Nature, 347, 339–340, 1990. 32395

Latham, J.: Amelioration of global warming by controlled enhancement of the albedo and longevity of low-level maritime clouds, Atmos. Sci. Lett., 3, 52–58, doi:10.1006/asle.2002.0048, 2002. 32395

Lenton, T. M. and Vaughan, N. E.: The radiative forcing potential of different climate geoengineering options, Atmos. Chem. Phys., 9, 5539–5561, doi:10.5194/acp-9-5539-2009, 2009. 32395

Niemeier, U., Schmidt, H., Alterskjaer, K., and Kristjánsson, J. E.: Solar irradiance reduction via climate engineering: impact of different techniques on the energy balance and the hydrological cycle, J. Geophys. Res.-Atmos., 118, 11905–11917, doi:10.1002/2013JD020445, 2013. 32398, 32403

Robock, A., Oman, L., and Stenchikov, G. L.: Regional climate responses to climate engineering with tropical and Arctic SO_2 injections, J. Geophys. Res., 113, D16101, doi:10.1029/2008JD010050, 2008. 32395

Robock, A., Marquardt, A., Kravitz, B., and Stenchikov, G.: Benefits, risks, and costs of stratospheric climate engineering, Geophys. Res. Lett., 36, L19703, doi:10.1029/2009GL039209, 2009. 32395

Schmidt, H., Alterskjær, K., Bou Karam, D., Boucher, O., Jones, A., Kristjánsson, J. E., Niemeier, U., Schulz, M., Aaheim, A., Benduhn, F., Lawrence, M., and Timmreck, C.: Solar irradiance reduction to counteract radiative forcing from a quadrupling of CO_2: climate responses simulated by four earth system models, Earth Syst. Dynam., 3, 63–78, doi:10.5194/esd-3-63-2012, 2012. 32395, 32396

Sillmann, J., Kharin, V. V., Zhang, X., Zwiers, F. W., and Bronaugh, D.: Climate extremes indices in the CMIP5 multimodel ensemble: Part 1. Model evaluation in the present climate, J. Geophys. Res.-Atmos., 118, 1716–1733, doi:10.1002/jgrd.50203, 2013. 32399

Taylor, K. E., Stouffer, R. J., and Meehl, G. A.: An overview of CMIP5 and the experiment design, B. Am. Meteorol. Soc., 93, 485–498, doi:10.1175/BAMS-D-11-00094.1, 2012. 32398

Tilmes, S., Fasullo, J., Lamarque, J.-F., Marsh, D. R., Mills, M., Alterskjaer, K., Muri, H., Kristjánsson, J. E., Boucher, O., Schulz, M., Cole, J. N. S., Curry, C. L., Jones, A., Haywood, J., Irvine, P. J., Ji, D., Moore, J. C., Karam, D. B., Kravitz, B., Rasch, P. J., Singh, B., Yoon, J.-H., Niemeier, U., Schmidt, H., Robock, A., Yang, S., and Watanabe, S.: The hydrological impact of climate engineering in the Geoengineering Model Intercomparison Project (GeoMIP), J. Geophys. Res.-Atmos., 118, 11036–11058, doi:10.1002/jgrd.50868, 2013. 32397

ACPD
14, 32393–32425, 2014

Climate extremes in climate engineering simulations

V. N. Aswathy et al.

Table 1. Climate extreme indices.

Index	Description	Index definition	Units
P90/P99	90th/99th percentile	90th/99th percentiles for given time period	mm day^{-1} or °C
P10/P1	10th/1st percentile	10th/1st percentiles for given time period	°C
CDD	Consecutive dry days index	Number of consecutive days where precipitation < 1 mm per time period	days year^{-1}
FD	Frost days index	Number of days per time period when TN < 0 °C	days year^{-1}
SU	Summer days index	Number of days per time period when TX > 25 °C	days year^{-1}

ACPD
14, 32393–32425, 2014

Table 2. Change in temperature and precipitation of 2060s relative to RCP4.5 2010s. "Tropical" refers to the entire area between 30° S and 30° N.

		Temperature (K)				Precipitation ($mm\,day^{-1}$)			
		Global	Land	Ocean	Tropical	Global	Land	Ocean	Tropical
RCP4.5	Mean	1.27	1.45	1.17	1.02	0.06	0.04	0.07	0.06
	P90	1.03	1.47	0.80	1.05	0.16	0.14	0.17	0.14
	P99	1.08	1.52	0.84	1.09	0.83	0.70	0.90	1.08
	P10	1.51	1.63	1.45	0.99	–	–	–	–
	P1	1.57	1.51	1.59	1.04	–	–	–	–
G3-SSCE	Mean	0.63	0.77	0.55	0.29	0.01	0.02	0.00	−0.02
	P90	0.53	0.89	0.34	0.28	0.02	0.08	−0.01	−0.06
	P99	0.54	0.88	0.36	0.26	0.14	0.33	0.04	−0.04
	P10	0.77	0.86	0.73	0.30	–	–	–	–
	P1	0.84	0.94	0.79	0.36	–	–	–	–
G3	Mean	0.58	0.65	0.53	0.40	0.01	0.00	0.01	−0.01
	P90	0.42	0.57	0.34	0.42	0.03	0.01	0.04	−0.01
	P99	0.41	0.54	0.34	0.42	0.22	0.19	0.24	0.19
	P10	0.79	0.88	0.73	0.38	–	–	–	–
	P1	0.86	0.90	0.84	0.40	–	–	–	–

ACPD
14, 32393–32425, 2014

Table 3. Change in temperature and precipitation of 2080s relative to 2060s.

		Temperature (in K)				Precipitation (in mm day^{-1})			
		Global	Land	Ocean	Tropical	Global	Land	Ocean	Tropical
RCP4.5	Mean	0.26	0.32	0.23	0.18	0.014	0.01	0.02	0.01
	P90	0.19	0.24	0.17	0.23	0.05	0.03	0.06	0.07
	P99	0.19	0.20	0.19	0.25	0.25	0.09	0.34	0.50
G3-SSCE	Mean	0.73	0.78	0.70	0.76	0.06	0.03	0.08	0.08
	P90	0.54	0.62	0.50	0.80	0.15	0.08	0.19	0.22
	P99	0.56	0.63	0.52	0.85	0.74	0.38	0.93	1.26
G3	Mean	0.87	0.99	0.80	0.72	0.06	0.05	0.07	0.07
	P90	0.74	1.06	0.56	0.76	0.16	0.16	0.16	0.17
	P99	0.78	1.13	0.60	0.80	0.71	0.55	0.80	1.01

ACPD
14, 32393–32425, 2014

Table 4. Comparison of G3/G3-SSCE 2060s relative to RCP4.5 2060s

		Temperature (in K)				Precipitation (in mm day^{-1})			
		Global	Land	Ocean	Tropical	Global	Land	Ocean	Tropical
G3-SSCE – RCP4.5	Mean	−0.64	−0.68	−0.62	−0.73	−0.05	−0.02	−0.07	−0.08
	P90	−0.54	−0.57	−0.46	−0.77	−0.14	−0.06	−0.18	−0.21
	P99	−0.54	−0.64	−0.48	−0.83	−0.69	−0.37	−0.86	−1.11
G3 – RCP4.5	Mean	−0.69	−0.79	−0.63	−0.62	−0.06	−0.05	−0.06	−0.08
	P90	−0.61	−0.89	−0.46	−0.63	−0.13	−0.13	−0.13	−0.16
	P99	−0.67	−0.98	−0.50	−0.67	−0.61	−0.51	−0.67	−0.89

ACPD
14, 32393–32425, 2014

Table 5. Change in CDD, FD and SU of 2060s realtive to RCP4.5 2010s.

	CDD (days year^{-1})				FD (days year^{-1})				SU (days year^{-1})			
	Global	Land	Ocean	Tropical	Global	Land	Ocean	Tropical	Global	Land	Ocean	Tropical
RCP4.5	−0.56	−1.8	0.12	1.44	−5.98	−6.57	−5.67	−0.36	11.25	9.20	12.34	26.8
G3-SSCE	−0.13	−0.68	−0.16	0.65	−3.30	−3.62	−3.13	−0.15	4.05	4.72	3.69	8.11
G3	−0.19	−0.88	0.17	0.80	−2.86	−2.74	−2.92	−0.10	4.75	3.79	5.26	11.76

ACPD
14, 32393–32425, 2014

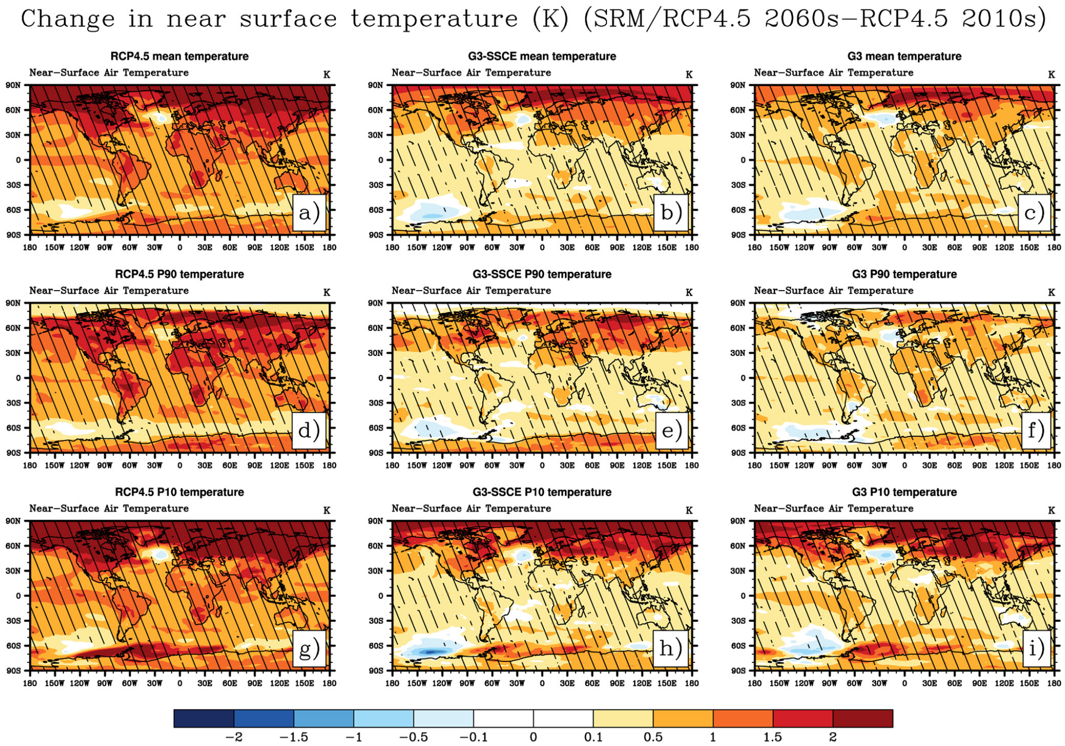

Figure 1. Multi-model mean change in near surface temperature (K) for RCP 4.5 (left panel), G3-SSCE (middle) and G3 (right panel) for 2060s relative to RCP4.5 2010s. **(a–c)** denote changes in mean values, **(d–f)** same as **(a–c)** but for the 90th percentile and **(g–i)** same as (**a–c**) but for the 10th percentile of the temporal distribution at each model grid point. Hatches denote regions where all the three models agree on the sign.

ACPD
14, 32393–32425, 2014

Climate extremes in climate engineering simulations

V. N. Aswathy et al.

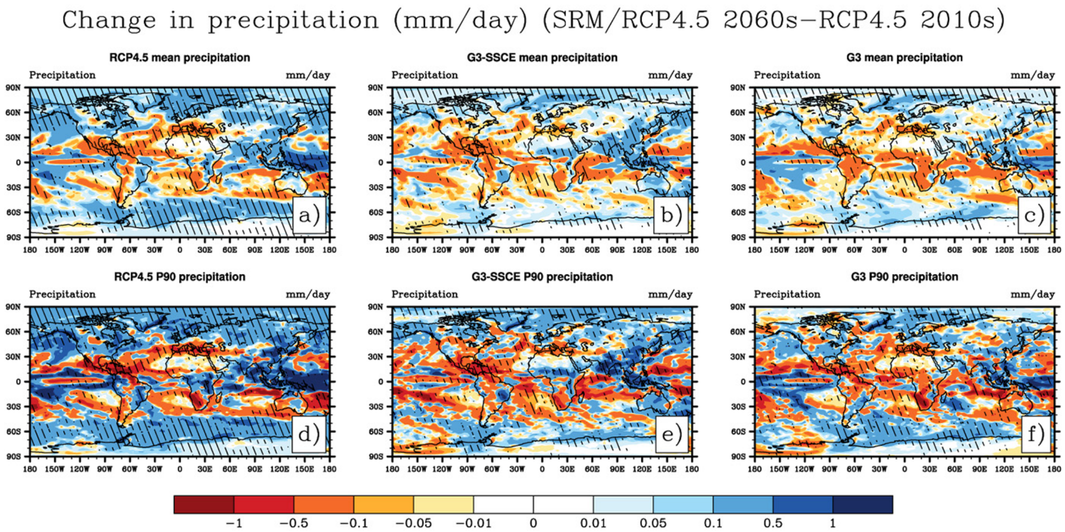

Figure 2. Multi-model mean change in precipitation (mm day^{-1}) for RCP 4.5 (left panel), G3-SSCE (middle) and G3 (right panel) for 2060s relative to RCP4.5 2010s. **(a–c)** denote changes in mean values, **(d–f)** same as **(a–c)** but for the 90th percentile of the temporal distribution at each model grid point. Hatches denote regions where models agree on the sign.

ACPD
14, 32393–32425, 2014

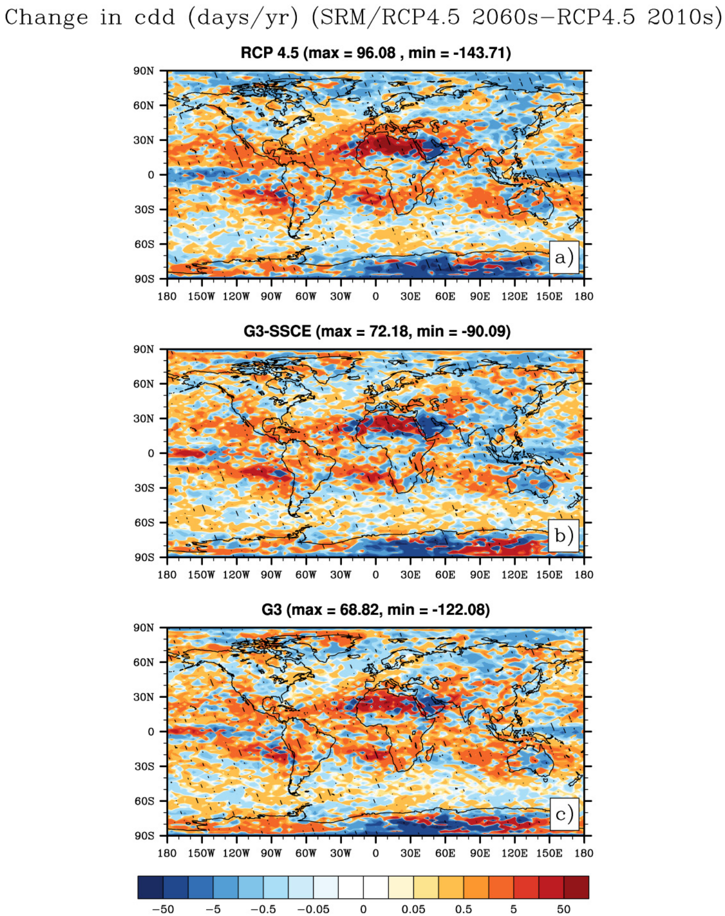

Figure 3. Multimodel ensemble mean of change in consecutive dry days RCP4.5 (top panel), G3-SSCE (middle) and G3 (bottom panel) for 2060s relative to RCP4.5 2010s. Hatches denote regions where all the three models agree on the sign.

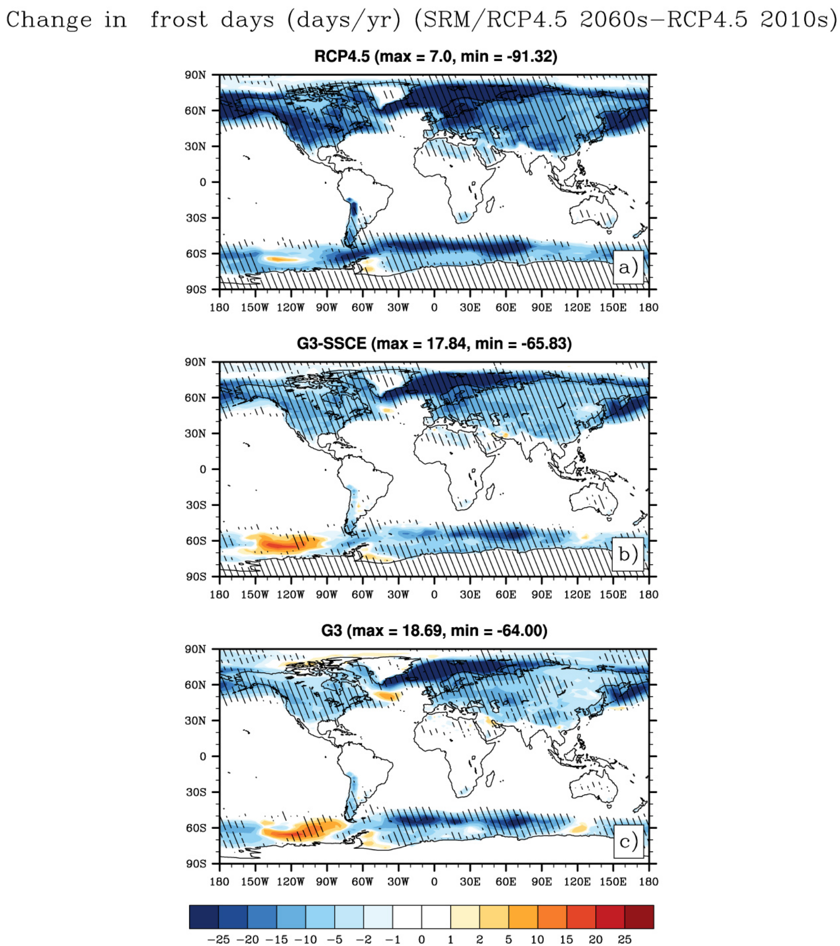

Figure 4. As in Fig. 3 but for Frost days. Hatches denote regions where all the three models agree on the sign.

ACPD
14, 32393–32425, 2014

Title Page
Abstract | Introduction
Conclusions | References
Tables | Figures
◀| |▶
◀ ▶
Back | Close
Full Screen / Esc
Printer-friendly Version
Interactive Discussion

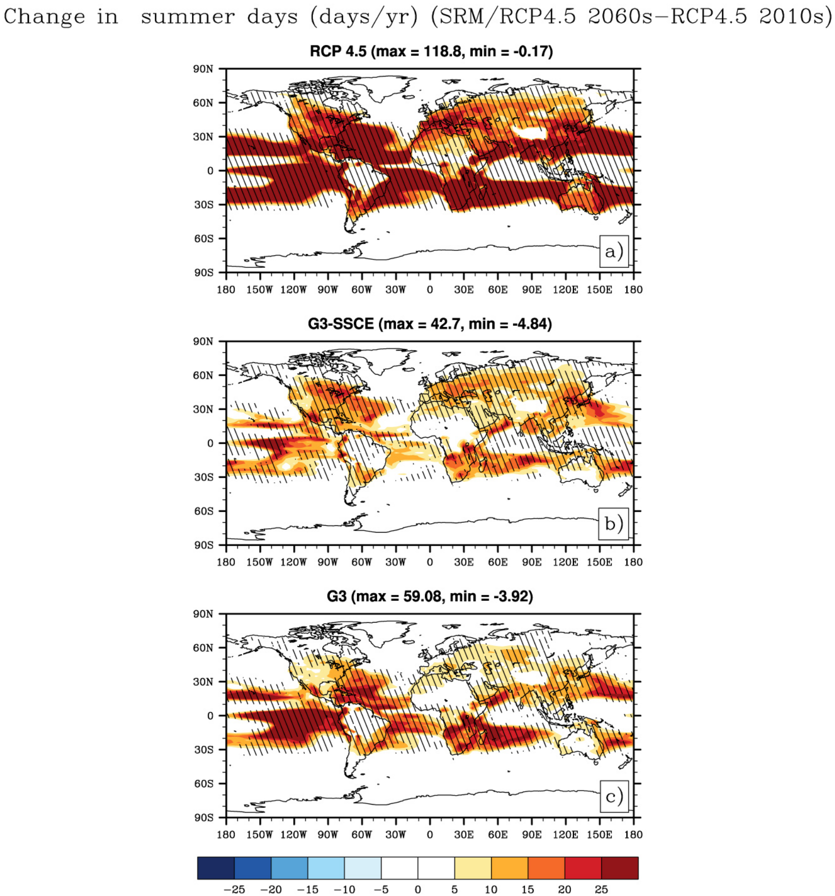

Figure 5. As in Fig. 3 but for Summer days. Hatches denote regions where all the three models agree on the sign.

ACPD
14, 32393–32425, 2014

Climate extremes in climate engineering simulations

V. N. Aswathy et al.

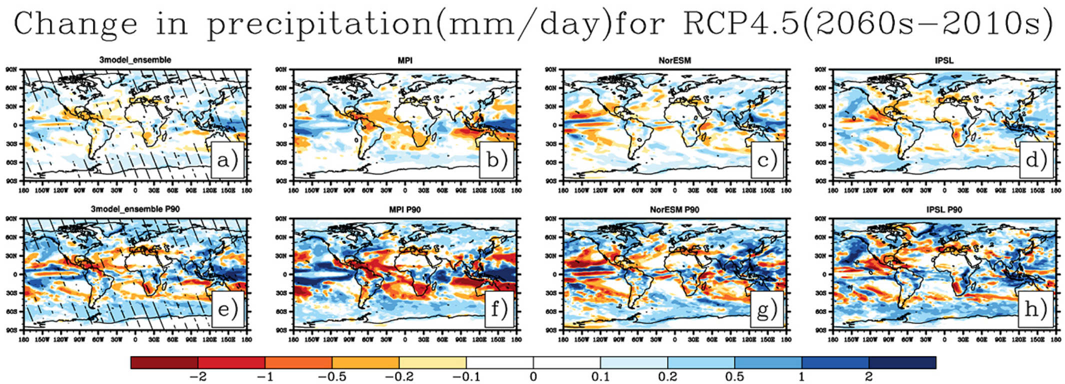

Figure 6. Change in precipitation (mm day^{-1}) for RCP4.5 of 2060s relative to 2010s. (**a** and **e**) show the multi-model ensemble average, **(b–d)** show the mean changes and **(f–h)** show the P90 changes of MPI-ESM, NorESM1-M and IPSL respectively. Hatches denote regions where all the three models agree on the sign.

ACPD
14, 32393–32425, 2014

ACPD
14, 32393–32425, 2014

Climate extremes in climate engineering simulations

V. N. Aswathy et al.

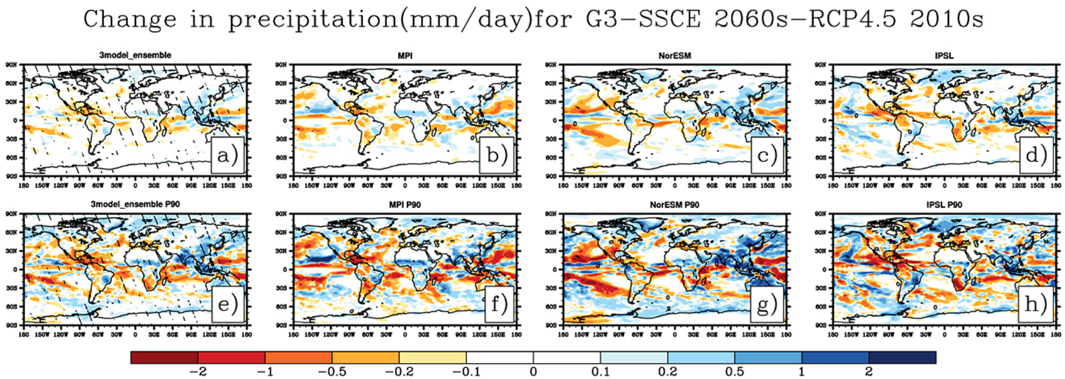

Figure 7. Same as in Fig. 6, but for G3-SSCE. Hatches denote regions where all the three models agree on the sign.

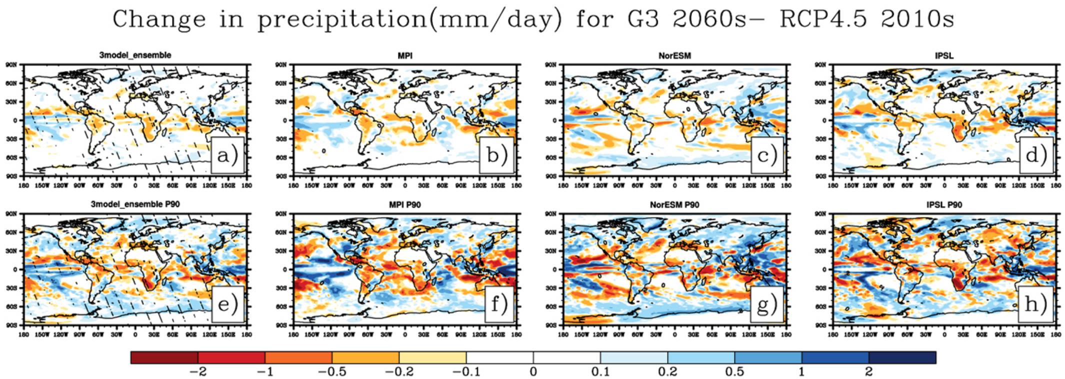

Figure 8. Same as in Fig. 6, but for G3. Hatches denote regions where all the three models agree on the sign.

ACPD
14, 32393–32425, 2014

Climate extremes in climate engineering simulations

V. N. Aswathy et al.